antibiotics

MDPI

Article

Poly(lactic acid)/Zinc/Alginate Complex Material: Preparation and Antimicrobial Properties

Marcin H. Kudzin *, Małgorzata Giełdowska, Zdzisława Mrozińska and Maciej Boguń

Lukasiewicz Research Network-Textile Research Institute, Brzezinska 5/15, 92-103 Lodz, Poland; malgorzata.gieldowska@iw.lukasiewicz.gov.pl (M.G.); zdzislawa.mrozinska@iw.lukasiewicz.gov.pl (Z.M.); maciej.bogun@iw.lukasiewicz.gov.pl (M.B.)

* Correspondence: marcin.kudzin@iw.lukasiewicz.gov.pl; Tel.: +48-42-6163121

Abstract: The aim of this study was to investigate an antimicrobial and degradable composite material consisting of melt-blown poly(lactic acid) nonwoven fabrics, alginate, and zinc. This paper describes the method of preparation and the characterization of the physicochemical and antimicrobial properties of the new fibrous composite material. The procedure consists of fabrication of nonwoven fabric and two steps of dip-coating modification: (1) impregnation of nonwoven samples in the solution of alginic sodium salt and (2) immersion in a solution of zinc (II) chloride. The characterization and analysis of new material included scanning electron microscopy (SEM), specific surface area (SSA), and total/average pore volume (BET). The polylactide/alginate/Zn fibrous composite were subjected to microbial activity tests against colonies of Gram-positive (*Staphylococcus aureus*), Gram-negative (*Escherichia coli*) bacterial strains, and the following fungal strains: *Aspergillus niger* van Tieghem and *Chaetomium globosum*. These results lay a technical foundation for the development and potential application of new composite as an antibacterial/antifungal material in biomedical areas.

Keywords: alginate; alginic acid; antibacterial activity; biodegradable composite; composite; melt-blown; nonwoven fabric; polymer; poly(lactide) PLA; zinc(II)chloride

Citation: Kudzin, M.H.; Giełdowska, M.; Mrozińska, Z.; Boguń, M. Poly(lactic acid)/Zinc/Alginate Complex Material: Preparation and Antimicrobial Properties. *Antibiotics* **2021**, *10*, 1327. https://doi.org/10.3390/antibiotics10111327

Academic Editor: Serena Riela

Received: 8 October 2021
Accepted: 27 October 2021
Published: 30 October 2021

1. Introduction

Wound healing is a dynamic and complex process (phases: hemostasis, inflammation, proliferation, and maturation) affected by several factors, which needs an appropriate surrounding to achieve accelerated healing [1]. Modern wound healing dressing should exhibit non-toxic and non-allergenic properties, be capable of maintaining high humidity at the wound site while removing excess exudate, antibacterial characteristics or at least impermeability to bacteria, enable gaseous exchange, and be cost effective [2–5]. These requirements are partly fulfilled by the physico-chemical properties of PLA (biocompatibility, biodegradability, mechanical strength) [6–15] and to a much larger extent by PLA-composites equipped with a wide spectrum of antimicrobial agents, including inorganic microbials [16,17].

Among the various inorganic bactericides applied in antibacterial polymers [18–37] increasing attention has focused on zinc salts [38], which is vitally essential for many biological processes [39], toxic to microbials and nontoxic to higher organisms [40], and a cheap and antibacterially efficient [41–47] inorganic antimicrobial. The zinc biochemistry and biology are determined by the complexation and hydration of zinc ions [48–54]. The zinc (II) coordination environment (tetrahedral vs. octahedral zinc complexes [55]) is limited in proteins to oxygen, nitrogen, and sulfur donors from the side chains of a few amino acids [31,33]. In living organisms, usually tetracoordinated Zn(II) is redox-inert since its standard reduction potential is negative ($Zn^{2+}(aq) + 2e^- \rightarrow Zn(s)$; Eo = −0.76V) [56].

Since an effective antibacterial PLA composite should exhibit prolonged antibacterial activity, a stable surface deposition/attachment of zinc to PLA presents a major problem.

Due to the low affinity of metallic cations to carboxylic ester bonds [57], PLA weakly binds zinc ions, and its antibacterial PLA-$Zn^{(2+)}$ composites require an interface covering layer with high affinity to copper. Such requirements fulfill alginates, biodegradable biopolymers [58–63] applied as a basis for drug delivery [64–78], tissue engineering [79–89], and wound dressings [90–98].

The role of alginate in antibacterial finishing of textiles was reviewed recently by Li et al. [99]. PLA-ALG have been investigated in a few papers for various applications [100–107].

The strong affinity of alginates to metal cations allows their application as antibacterial hybrids (e.g., [108–111]). ALG-$Zn^{(2+)}$ complexes have been described in 792 papers [112] (e.g., [113–124]).

As part of our investigations focused on the functionalization of textile materials [125–131], we propose the use of an alginate film covering the PLA matrix (PLA-ALG), which, after adding copper salts, was cross-linked to form an outer space coating with strongly bound copper ions (Figure 1). Such a PLA-Alg-$Zn^{(2+)}$ composite slowly releases zinc ions, ensuring its long-lasting antibacterial activity (Figure 2).

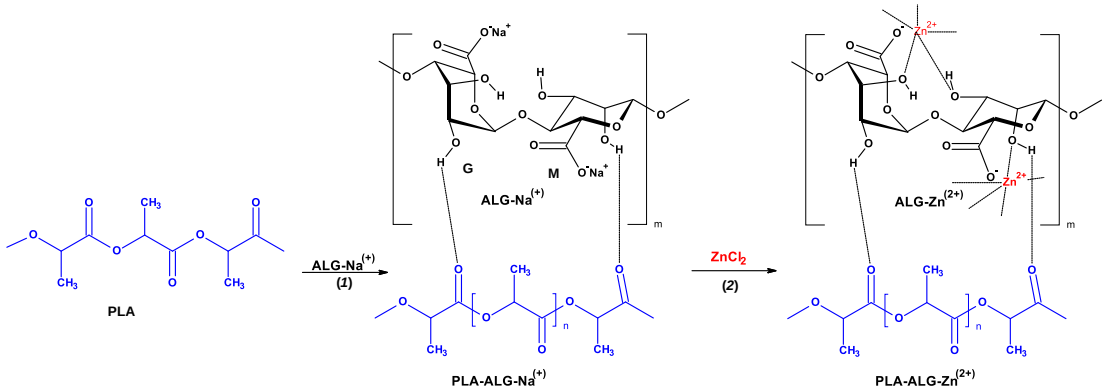

Figure 1. The reactions involved in the preparation of fibrous composite: PLA→PLA-ALG-$Na^{(+)}$ →PLA-ALG-$Zn^{(2+)}$. The structure of alginate is presented as a linear copolymer –[GM]n- with homopolymeric blocks of (1-4)-linked β-D-mannuronate (M) and its C-5 epimer α-L-guluronate (G) residues.

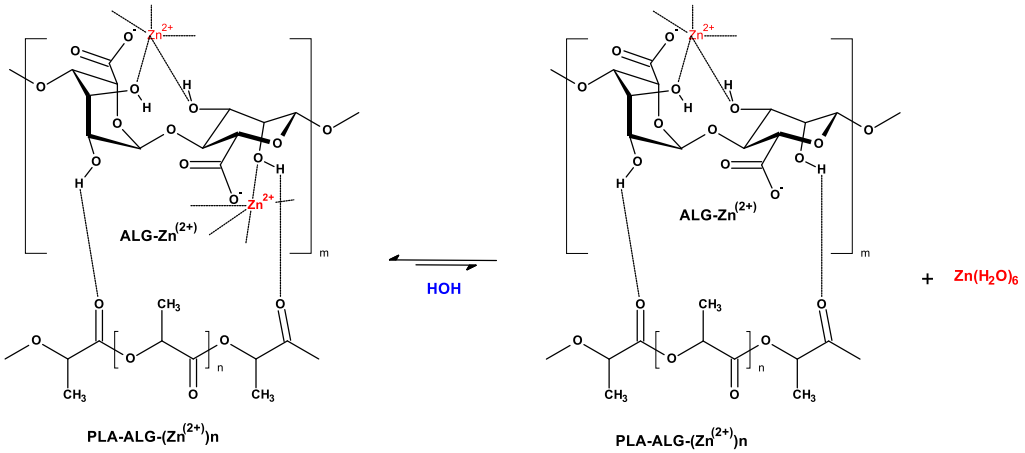

Figure 2. The reactions involved in the release of zinc ion from the PLA-ALG-$Zn^{(2+)}$ composite in an aqueous environment.

2. Materials and Methods

2.1. Materials

- Alginic acid sodium salt, C5H7O4COONa (CAS: 9005-38-3) were purchased from Millipore Sigma (St. Louis, MO, USA);

- Bacterial strains: *Escherchia coli* (ATCC 25922) and *Staphylococcus aureus* (ATCC 6538) were purchased from Microbiologics (St. Cloud, MN, USA);
- Fungal strains: *Aspergillus niger* van Tieghem (ATCC 6275) and *Chaetomium globosum* (ATCC 6205) were purchased from Microbiologics.
- Poly(lactic acid) was provided by NatureWorks LLC (Minnetonka, MN, USA), type Ingeo™ 3251D, with an MFR value of 30–40 g/10 min (at 190 °C/2.16 kg);
- Zinc (II) chloride, ZnCl2, 98% (CAS: 7646-85-7) was purchased from Millipore Sigma.

2.2. Methods

2.2.1. Preparation of Fibrous Material—Melt-Blown Process

The poly(lactic acid) melt-blown nonwoven fabrics with a basis weight of 250 g/m^2 were produced by using a one-screw laboratory extruder (Axon, Limmared, Sweden). The extruder head has 30 holes with a 0.25 mm die orifice diameter each. The polylactide (PLA) granulate for melt blowing was dried at 80 °C to constant weight. The process parameters of melt blowing are given in Table 1.

Table 1. Processing parameters of the melt blown process.

Parameter	Value
Extruder screw zone temperatures	195–260 °C
Extruder head temperature	260 °C
Air temperature	260 °C
Air flow rate	8 m^3/h
The area density of nonwoven fabric	250 g/m^2

2.2.2. Modification—Dip-Coting

The PLA melt-blown nonwoven fabrics samples were modified by dip-coting, a two-step method: (1) impregnation in the solution of alginic acid sodium salt and (2) immersion in the solution of zinc (II) chloride. Samples of PLA nonwoven fabric were impregnated in a homogeneously dispersed polysaccharide solution (0.5%) for 1 min (sample: PLA-Alg-$Na^{(+)}$), then each sample was immediately transferred into two different aqueous solutions of zinc (II) chloride and re-immersed for 1 min (sample PLA-Alg-$Zn^{(2+)}$-1 re-immersed in 5% $ZnCl_2$ solution and sample PLA-Alg-$Zn^{(2+)}$-2 re-immersed in 10% $ZnCl_2$ solution). Then, the samples were squeezed and dried for 5 h at 50 °C to constant weight. The modifier components are given in Table 2.

Table 2. Composition of the dip-coating solution of poly(lactide) (PLA) surface modifier (%).

Sample Assignments/Name	Mixture Components of Film-Forming Material (%)		
	Sodium Alginate Solution	Zinc (II) Chloride Solutions	
	0.5%	5%	10%
PLA	–	–	–
PLA-Alg-$Na^{(+)}$	+	–	–
PLA-Alg-$Zn^{(2+)}$-1	+	+	–
PLA-Alg-$Zn^{(2+)}$-2	+	–	+

2.2.3. Morphological and Structural Characterization—Scanning Electron Microscopy

Examination of the microscopic structures was carried out using a HITACHI S-4700 scanning electron microscope equipped with a Thermo NORAN EDS X-ray microanalyzer. The topographic analysis of the tested samples was carried out in low vacuum with a beam energy of 10 kV and at magnifications of 800× and 1600×.

2.2.4. Morphological and Structural Characterization—Specific Surface Area

The specific surface area was determined by the Brunauer, Emmet, and Teller method (BET). Measurements were carried out on an Autosorb-1 apparatus (Quantachrome Instruments, Boynton Beach, FL, USA), using nitrogen as a sorption agent and an adsorption isotherm at 77 K. In each experiment, approximately 1–2 g of a given sample were weighed and used. Prior to the analysis, the samples were dried in 105 °C for 24 h and degassed at room temperature. Measurements were made in duplicate, and the results were presented as a mean value.

2.2.5. Morphological and Structural Characterization—Contact Angle and Wettability

Surface wettability was determined by static measurements of the water wetting angle. The wetting angle was measured by the "sitting droplet" method using a drop shape analysis (DSA) system DSA 10 Mk2 (Kruss GmbH, Hamburg, Germany). Water drops of 0.25 µL were applied to each clean and dry sample. The apparent contact angle was calculated as the average of 10 measurements [132].

2.2.6. Chemical Characterization—Atomic Absorption Spectrometry with Flame Excitation

Determination of the zinc content in PLA-Alg-$Zn^{(2+)}$ composites was assessed by the FAAS method. The previous sample was mineralized (Figure 3) using a single-module Magnum II microwave mineralizer from Ertec (Wroclaw, Poland), in similar way as was described earlier [133].

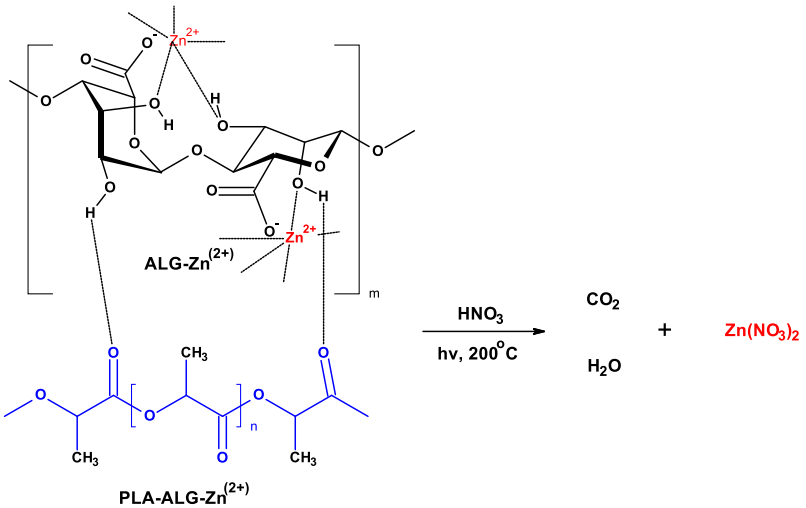

Figure 3. Mineralization of PLA-Alg-$Zn^{(2+)}$.

Determination of the zinc (II) ions was performed by atomic absorption spectrometry with flame excitation using a Thermo Scientific Thermo Solar M6 (LabWrench, Midland, ON, Canada) spectrometer equipped in similar way as was described earlier [133,134]. Measurements were made in triplicate and the results were presented as a mean value.

2.2.7. Antimicrobial Activity

The antibacterial activity of PLA-Alg-$Zn^{(2+)}$ material was assessed according to standard PN-EN ISO 20645:2006 [135] against a representative colony of Gram-negative and Gram-positive bacteria (*Escherchia coli*/*Staphylococcus aureus*). The antifungal activity of composites was tested according to PN–EN 14119:2005 [136] against an *Aspergillus niger* van Tieghem (ATCC 6275) and *Chaetomium globosum* (ATCC 6205). All tests (modified samples and unmodified PLA) were carried out in duplicate.

3. Results and Discussion

3.1. Scanning Electron Microscopy

The presented SEM images illustrate changes in the morphology of the fiber surface of the investigated samples. These changes are the result of modification of PLA nonwoven fabric with sodium salt solution of alginic acid and $ZnCl_2$.

The SEM image of the unmodified nonwoven fabric presents a mesh of randomly oriented fibers with interconnected pores and a comparatively smooth surface (Figure 4). Modification of the nonwoven fabric with sodium alginate solution (PLA→PLA-ALG$^{(-)}$ Na$^{(+)}$) induced the formation of a film on the fiber surface, during which the PLA fibrous structure serves as a matrix for a deposited alginate, presumably by the formation of hydrogen bonds between the HO group of alginate and the carbonyls of the carboester functions of PLA. This modification slightly affected the overall morphology of the formed composite surface, maintaining the fibrous structure of the PLA→PLA-ALG$^{(-)}$Na$^{(+)}$ composites but with more irregular shapes and less visible pores. Additionally, agglomerates of sodium alginate (ALG-Na$^{(+)}$) can be seen on single fibers of PLA-ALG^{-}Na$^{(+)}$ (Figure 5). Further modification of the temporary composite PLA-ALG$^{(-)}$Na$^{(+)}$ with $ZnCl_2$, (PLA-ALG$^{(-)}$ Na$^{(+)}$→PLA-ALG-Zn$^{(2+)}$) led to immense changes in its morphology, probably due to the formation of interchain complexes PLA^1-ALG^1-Zn$^{(2+)}$-ALG^2-PLA^2 (PLA^1-ALG$^{1(-)}$Na$^{(+)}$→PLA^1-ALG^1-Zn$^{(2+)}$→PLA^1-ALG^1-Zn$^{(2+)}$-ALG^2-PLA^2). Therefore, the fibrous structure of the resulting composite was largely deformed with an increase of surface roughness, with multiple zinc agglomerates (Figure 6), resembling a polymer film, with integrated PLA fibers.

Figures 7–9 present example of the EDS spectra for PLA, PLA-Alg-Na$^{(+)}$, and PLA-Alg-Zn$^{(2+)}$ (10%) samples (EDS data are presented as a plot of the peak intensity versus energy (keV)). Table 3 shows the chemical composition of the tested materials, obtained by quantitative analysis using EDS X-ray microanalysis. The table presents the averaged results obtained from five measurement points.

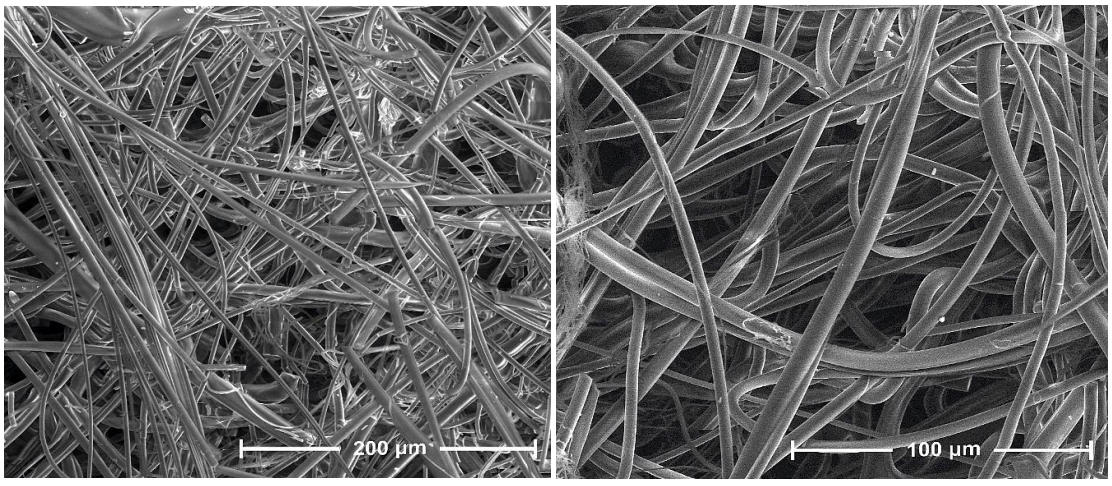

(**a**) (**b**)

Figure 4. SEM images of PLA, magnification: (**a**) 800× and (**b**) 1600×.

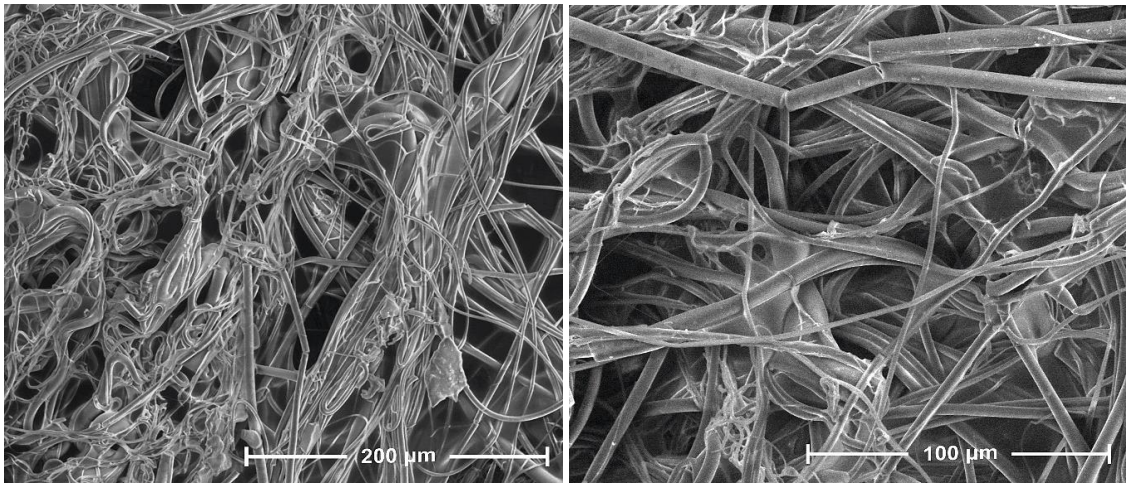

(**a**) (**b**)

Figure 5. SEM images of PLA-ALG-$Na^{(+)}$, magnification: (**a**) 800× and (**b**) 1600×.

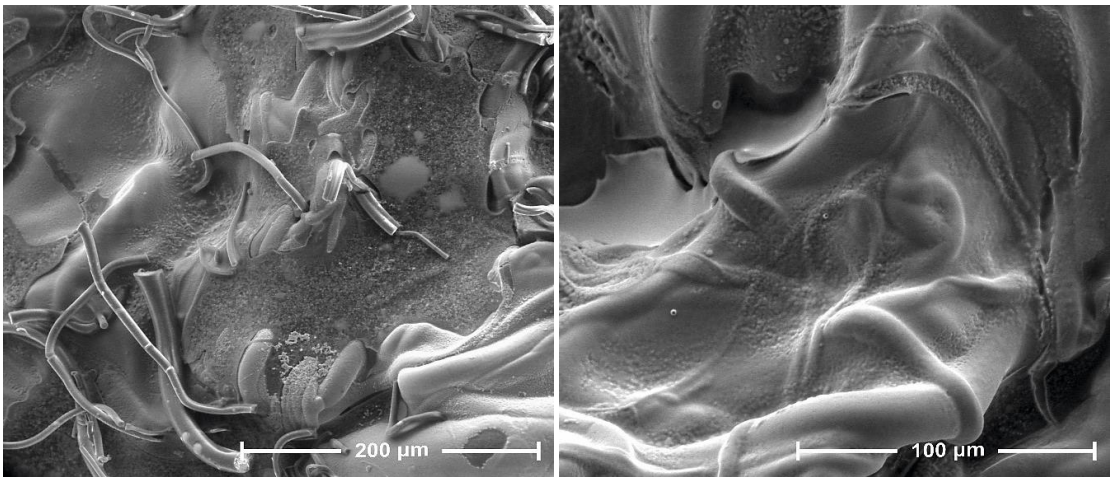

(**a**) (**b**)

Figure 6. SEM images of PLA-ALG-$Zn^{(2+)}$, magnification: (**a**) 800× and (**b**) 1600×.

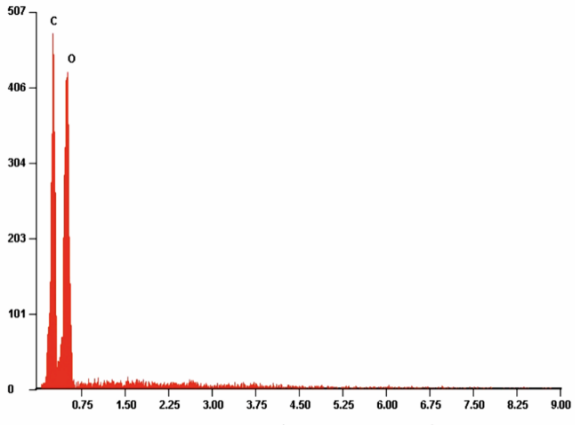

Figure 7. Example of the energy-dispersive X-ray spectroscopy (EDS) spectrum of PLA nonwoven fabric.

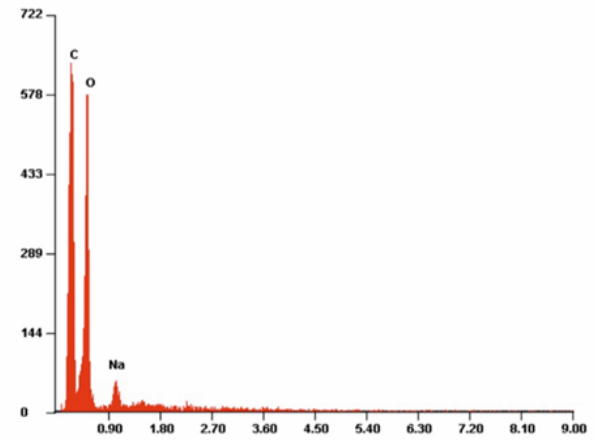

Figure 8. Example of the energy-dispersive X-ray spectroscopy (EDS) spectrum of PLA-ALG-$Na^{(+)}$.

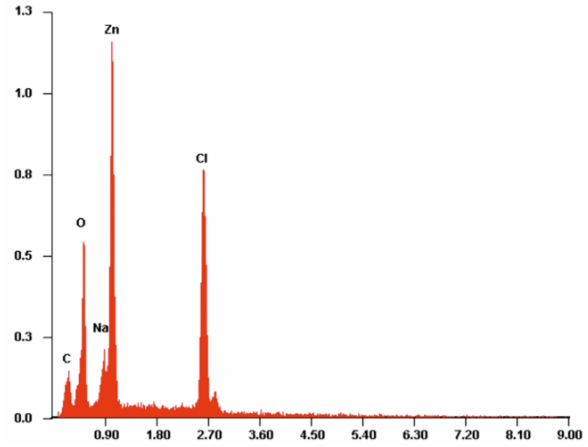

Figure 9. Example of the energy-dispersive X-ray spectroscopy (EDS) spectrum of PLA-ALG-$Zn^{(2+)}$.

Table 3. Quantitative results of the EDS analysis of PLA, PLA-ALG-$Na^{(+)}$, and PLA-ALG-$Zn^{(2+)}$.

PLA					
Atom	C	O			
At. %	54.70	45.30			
Std. dev.	0.18	0.18			
Wt. %	47.55	52.46			
Std. dev.	0.18	0.18			
PLA-ALG-$Na^{(+)}$					
Atom	C	O	Na		
At. %	54.42	43.93	1.65		
Std. dev.	1.61	2.55	0.03		
Wt. %	45.45	52.09	2.47		
Std. dev.	0.54	0.13	0.29		
PLA-ALG-$Zn^{(2+)}$					
Atom	C	O	Na	Zn	Cl
At. %	31.31	34.05	3.42	14.22	17.01
Std. dev.	1.21	3.58	0.76	0.52	1.29
Wt. %	14.62	21.18	4.61	36.14	23.45
Std. dev.	2.08	2.38	0.88	1.52	4.13

When analyzing the spectrum in Figure 7, it can be observed that the sample contains elements characteristic for polylactide, that is, carbon and oxygen. Whereas the PLA-

ALG-$Na^{(+)}$ sample, because of the modification with sodium alginate, is characterized by the presence of an additional peak, derived from Na atoms (Figure 8). Additionally, modification of PLA-ALG-$Na^{(+)}$ nonwoven fabric with zinc (II) chloride contributed to the presence of further peaks, originating from zinc and chloride. The presence of chloride is confirmed by the content of NaCl in the samples.

Quantitative EDS analysis showed that modification of PLA nonwoven fabric with sodium alginate did not significantly change the carbon and oxygen contents of the samples. Slight decreases in the content of these elements were observed: about 0.28 at. % and about 1.38 at. % for carbon and oxygen, respectively. Additionally, small concentrations of sodium (1.65 at %) were noted for the PLA-ALG-$Na^{(+)}$ sample. The EDS results for the samples modified with $ZnCl_2$ show that the content of Zn and Cl in the samples increased with the increasing chloride concentration. However, because it showed the best antibacterial and antifungal properties, the results are presented for the PLA-ALG-$Zn^{(2+)}$ sample (10%). We can observe that because of the rapid cross-linking of the sample surface and the formation of a kind of film on the surface, the sodium content increased twice, compared to the PLA-ALG-$Na^{(+)}$ sample. On the other hand, the high content of zinc (14.22%) confirms that the agglomerates shown in the photos are agglomerates of a divalent metal (Figure 9). Moreover, it can be seen that when the samples were modified with $ZnCl_2$, the carbon and oxygen content decreased significantly (by 23.39 at. % and 11.26 at. %, respectively). A high value of standard deviation indicates an irregular distribution of the chemical components.

3.2. Specific Surface Area

The specific surface area [m^2/g] and total pore volume [cm^3/g] of the composites are presented in Table 4.

Table 4. The specific surface area and total pore volume for unmodified PLA nonwoven and PLA-ALG-$Zn^{(2+)}$ composites.

Sample Name	Specific Surface Area [m^2/g]	Total Pore Volume [cm^3/g]
PLA	0.221 ± 0.03	9.10×10^{-4}
PLA-Alg-$Na^{(+)}$	0.587 ± 0.03	1.64×10^{-3}
PLA-Alg-$Zn^{(2+)}$-1	0.521 ± 0.02	2.75×10^{-3}
PLA-Alg-$Zn^{(2+)}$-2	0.833 ± 0.03	3.09×10^{-3}

The results of the specific surface area and the total pore volume measurements correspond to our previous studies [111]. The modification of poly(lactic acid) (PLA) nonwoven fabric with alginate (PLA-Alg-$Na^{(+)}$) and zinc (II) chloride (PLA-Alg-$Zn^{(2+)}$-1/PLA-Alg-$Zn^{(2+)}$-2) leads to significant growth of the specific surface area (BET). The BET of the poly(lactic acid) sample was equal to 0.221 [m^2/g]. The impregnation of unmodified PLA nonwoven fabric in the solution of alginic acid sodium salt resulted in an increase in the value of the specific surface area (0.58 [m^2/g]). The dip-coating two-step modification, i.e., impregnation in a solution of alginic acid sodium salt and immersion in a $ZnCl_2$ solution (5%/10%), caused an even further increase in BET to 0.5211 and 0.8331 m^2/g, respectively. The increase of the observed specific surface area for the modified samples (PLA-Alg-$Na^{(+)}$/PLA-Alg-$Zn^{(2+)}$-1/PLA-Alg-$Zn^{(2+)}$-2) may be related with their higher mesoporosity. Higher mesoporosity was confirmed by the total pore volume, which increased from 9.102×10^{-4} cm^3/g for the PLA nonwoven fabric to 1.64×10^{-3} cm^3/g for PLA-Alg-$Na^{(+)}$, 2.750×10^{-3} cm^3/g for PLA-Alg-$Zn^{(2+)}$-1, and 3.093×10^{-3} cm^3/g for PLA-Alg-$Zn^{(2+)}$-2.

3.3. Contact Angle and Wettability

The analysis of the contact angle enabled an assessment of the wettability of the surfaces of the tested materials. The results demonstrated that PLA and PLA-ALG $Zn^{(2+)}$ nonwoven fabrics were characterized by a hydrophobic character of the surface, for which

the average contact angle was 122.79° and 114.98°, respectively (Figure 10a,c). In contrast, the modification with sodium alginate changed the character of the material surface, which became hydrophilic with an average contact angle of 45.67° (Figure 10b).

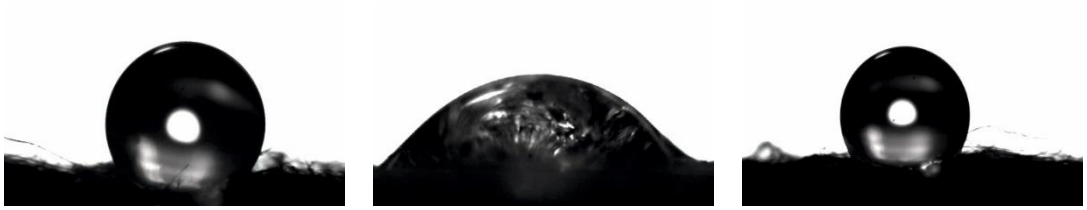

(**a**) (**b**) (**c**)

Figure 10. Contact angle images for: (**a**)—PLA, (**b**)—PLA-ALG-$Na^{(+)}$, (**c**)—PLA-ALG-$Zn^{(2+)}$.

As shown in Figures 10 and 11, modification of PLA nonwoven fabric with sodium alginate significantly changed the nature of the nonwoven fabric surface from hydrophobic to hydrophilic. This is due to the presence of the Na^+ ions contained in alginate, which make it soluble in water. On the other hand, another modification with $ZnCl_2$ resulted in substitution of sodium ions with divalent metal ions (Zn^{2+}), thanks to which the crosslinking process occurred on the surface and alginate covering fibers became insoluble in water. This changed the nature of the nonwoven surface from hydrophilic to hydrophobic again. However, it is characterized by lower surface hydrophobicity than the PLA nonwoven fabric, due to the Na^+ ions present on the surface in small amounts, which was confirmed by SEM-EDS analysis.

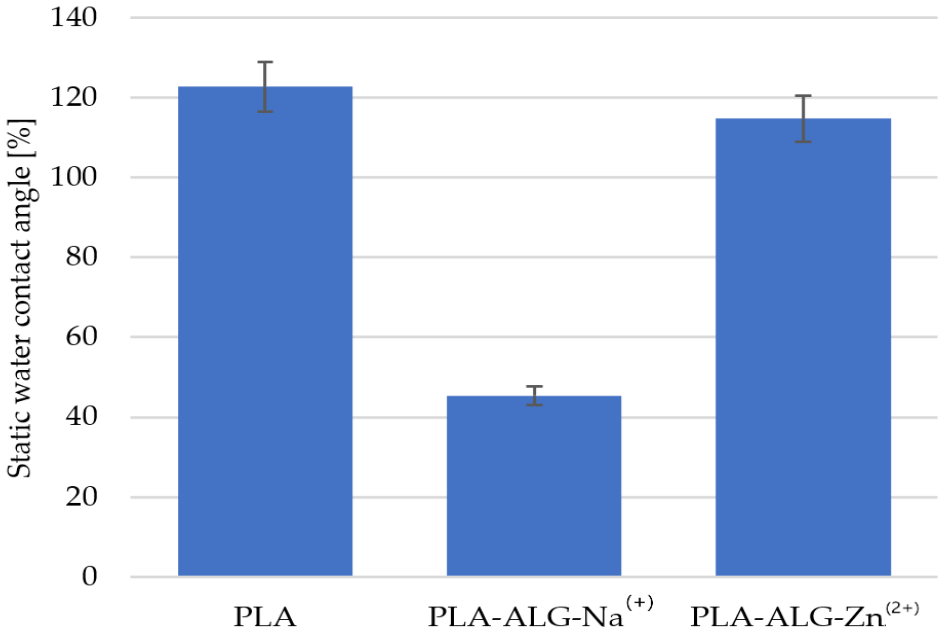

Figure 11. The static water contact angle of PLA and its composites.

3.4. Flame Atomic Absorption Spectrometry

Determination of the metal concentration in the PLA-Alg-$Zn^{(2+)}$ samples was assessed by the FAAS spectrometry, and the results are shown in Table 5.

Table 5. Zinc concentration in PLA-Alg-$Zn^{(2+)}$ samples.

Sample	Zn Concentration [g/kg]
PLA	0.003
PLA-Alg-$Na^{(+)}$	0.003
PLA-Alg-$Zn^{(2+)}$-1	11.55
PLA-Alg-$Zn^{(2+)}$-2	39.71

The results of the determination of the zinc concentration in PLA-Alg-$Zn^{(2+)}$ samples show that the metal content in complex materials depends on the variant of applied modifier dip-coating solution and type of solution of Zinc (II) chloride (Table 5). The higher concentration of the used zinc (II) chloride solutions (10%) resulted in the higher content of the metal on PLA-Alg-$Zn^{(2+)}$-2 material (39.71 g/kg), and the lower concentration of zinc (II) chloride (5%) gave a relatively lower content of Zn in the sample (PLA-Alg-$Zn^{(2+)}$-1—11.55 g/kg). Additionally, the FAAS spectrometry measurements also indicate that the distribution of zinc in the material is quite uniform (approximately 7.5%).

3.5. Antimicrobial Activity—Disc-Diffusion Assay

The antimicrobial activity of PLA-Alg-$Zn^{(2+)}$ composites was investigated by the disk diffusion method using Gram-negative (*E. coli*) and Gram-positive (*S. aureus*) bacteria (Table 6, Figure 12) and representative fungus species: *Aspergillus niger* and *Chaetomium globosum* (Table 7, Figure 13).

Control samples as unmodified PLA and modified by alginic acid sodium salt material (PLA-Alg-$Na^{(+)}$) exhibited strong growth of bacterial and fungal colonies covering the entire surface of the samples placed on Petri dishes (Figures 12a,c and 13a,c). Poly(lactic acid) material functionalized with a zinc/alginate complex, regardless of the metal concentration in PLA-Alg-$Zn^{(2+)}$ composites in the range from 11 to 39 [g/kg] (Table 5), showed an inhibitory effect against *S. aureus* bacteria and fungus species expressed by zones of inhibition and no visible growth on/under the samples (Tables 6 and 7). The increase of the zinc concentration in PLA-Alg-$Zn^{(2+)}$ composites caused an increase of the antimicrobial properties of the material. The PLA-Alg-$Zn^{(2+)}$-2 (39 [g/kg] of Zn) sample showed antimicrobial properties for all variants of the tested microorganisms (Figures 12b,d and 13b,d). The results obtained in accordance with the EN-ISO 20645:2006 and EN 14119:2005 standards confirm the antimicrobial protection of PLA-Alg-$Zn^{(2+)}$ complexes against various microorganisms [135,136].

Table 6. Antibacterial activity results according to standards EN-ISO 20645:2006 of PLA-Alg-$Zn^{(2+)}$ composites [135].

Sample	Average Inhibition Zone (mm)	
	E. coli	***S. aureus***
PLA nonwoven	0	0
PLA-Alg-$Na^{(+)}$	0	0
PLA-Alg-$Zn^{(2+)}$-1	0	>1
PLA-Alg-$Zn^{(2+)}$-2	>1	>1
Concentration of inoculum [CFU/mL]: *E. Coli*—1.8×10^8, *S. Aureus*—1.6×10^8		

Table 7. Antifungal activity results according to standards EN 14119:2005 of PLA-Alg-$Zn^{(2+)}$ composites [136].

Sample	Average Inhibition Zone (mm)		Visual Evaluation
	A. niger	*C. globosum*	
PLA nonwoven PLA-Alg-$Na^{(+)}$	0	0	Visible, strong growth on/under the sample
PLA-Alg-$Zn^{(2+)}$-1 PLA-Alg-$Zn^{(2+)}$-2	<1	<1	No visible growth on/under the sample
Concentration of inoculum [CFU/mL]: *A. niger*—2.8×10^6, *C. globosum*—2.2×10^6			

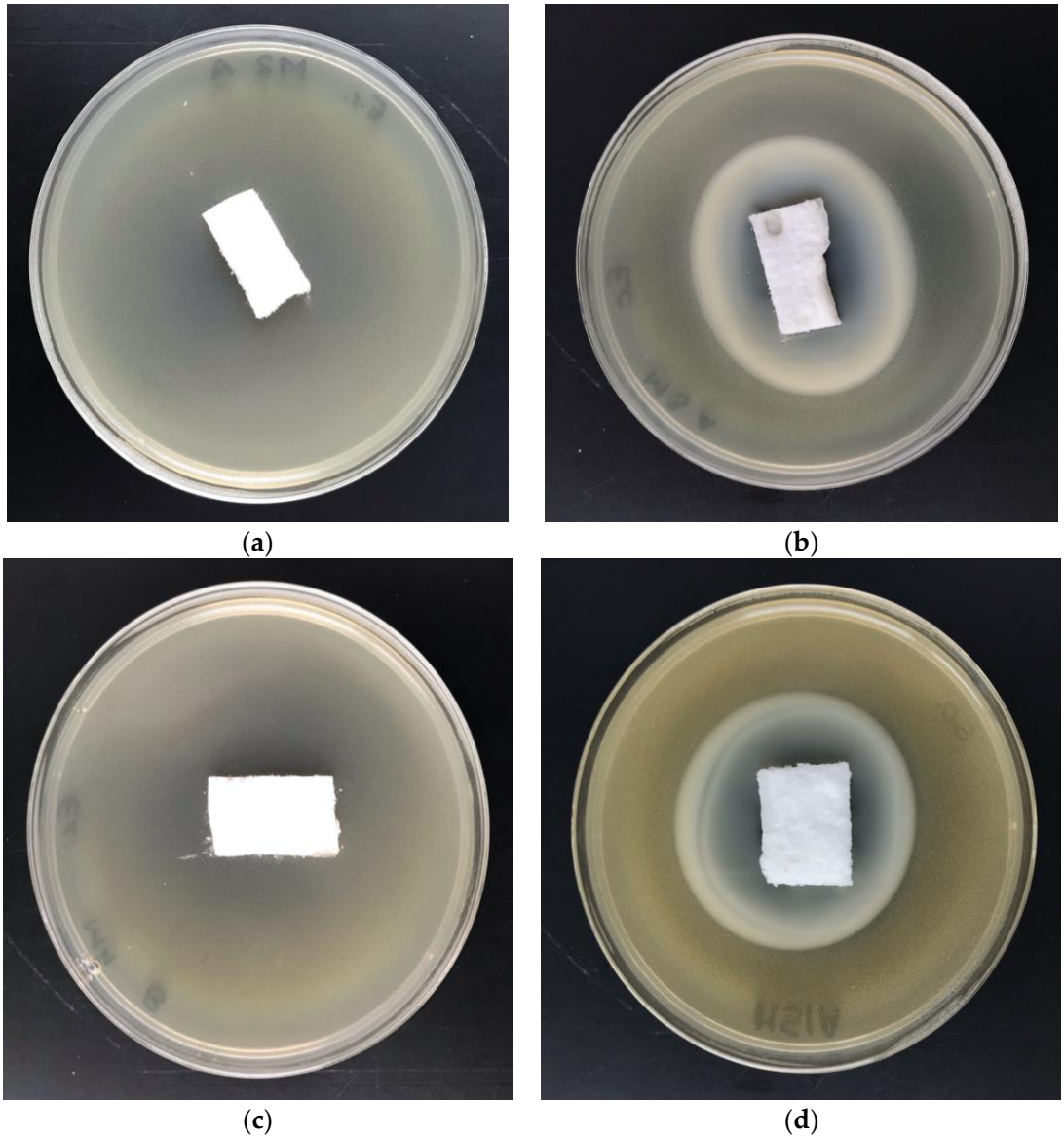

Figure 12. Zone of inhibition test results on Petri dishes showing antibacterial activity: (**a**,**b**)—*E. coli*; (**c**,**d**)—*S. aureus*; (**a**,**c**) Control: unmodified PLA nonwoven fabric, (**b**,**d**) Sample: PLA-ALG-$Zn^{(2+)}$.

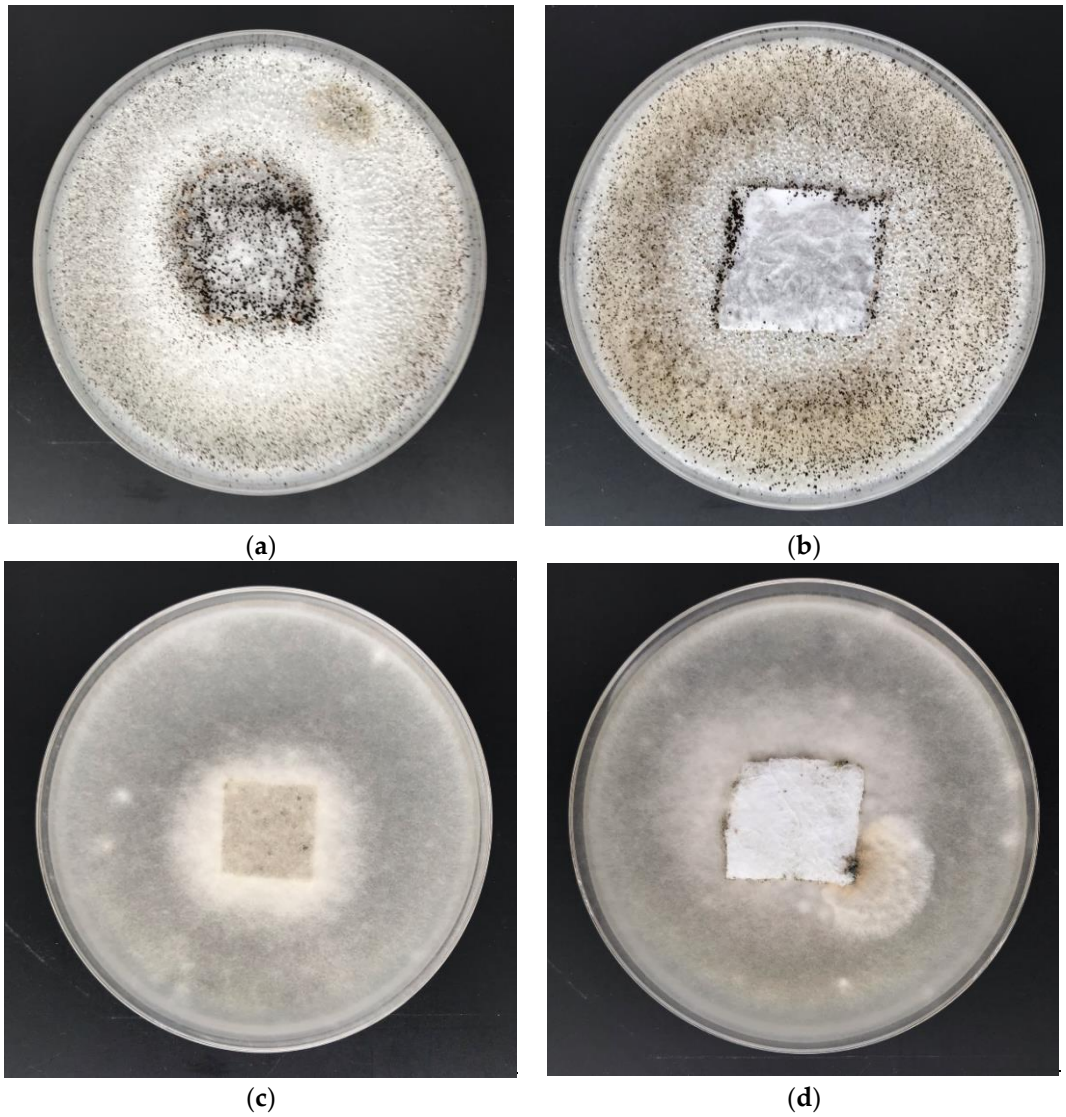

Figure 13. Zone of inhibition test results on Petri dishes showing antifungal activity: (**a**,**b**)—*A. niger*; (**c**,**d**)—*C. globosum*; (**a**,**c**)—Control: unmodified PLA nonwoven fabric; (**b**,**d**)—Sample: PLA-ALG-$Zn^{(2+)}$ material.

4. Conclusions

In this study, we developed and characterized a complex material consisting of alginic acid sodium salt, poly(lactide), and zinc (II) chloride. PLA-ALG-$Zn^{(2+)}$ composite was fabricated from biodegradable PLA polymer by the melt-blown method, and then the obtained fibrous material was modified by dip-coating, using alginic acid sodium salt and zinc (II) chloride. Structural characterization of the new material was achieved by scanning electron microscopy (SEM), and determination of the specific surface area and wettability. The chemical compositions of the PLA-Alg-$Zn^{(2+)}$ composites were identified using energy-dispersive X-ray spectroscopy EDS (C, O, Zn surface analysis) and atomic absorption spectrometry with flame excitation (Zn content in bulk). The obtained complex material exhibited an antimicrobial in vitro action against representative bacteria: *Escherichia coli* and *Staphylococcus aureus*, and fungus species: *Chaetomium globosum* and *Aspergillus niger*. From the point of view of our previous work, these results are promising regarding the material's applicability in different fields of materials science in the medical or healthcare industry.

Author Contributions: M.H.K. developed the concept and designed experiments, performed experiments, analyzed data, and wrote the paper; Z.M. and M.G. performed the experiments; M.B. co-authored of the concept and participated in the publication preparation. All authors have read and agreed to the published version of the manuscript.

Funding: This research was funded by the Polish Ministry of Science and Higher Education within statutory research work carried out at the The Lukasiewicz Research Network -Textile Research Institute, Lodz, Poland.

Acknowledgments: The authors would like to thank Sylwia Dziegieć, for providing the structural characterization.

Conflicts of Interest: The authors declare no conflict of interest.

References

1. Nethi, S.K.; Das, S.; Patra, C.R.; Mukherjee, S. Recent advances in inorganic nanomaterials for wound-healing applications. *Biomater. Sci.* **2019**, *7*, 2652–2674. [CrossRef] [PubMed]
2. Jones, V.; Grey, J.G.; Harding, K.G. Wound dressings. *BMJ* **2006**, *332*, 707–780. [CrossRef] [PubMed]
3. Dhivya, S.; Padma, V.V.; Santhini, E. Wound dressings—A review. *BioMedicine* **2015**, *5*, 24–28. [CrossRef] [PubMed]
4. Ghomi, E.R.; Khalili, S.; Khorasani, S.N.; Neisiany, R.E.; Ramakrishna, S. Wound dressings: Current advances and future directions. *J. Appl. Polym. Sci.* **2019**, *136*, 47738. [CrossRef]
5. Pandey, A.K.; Dwivedi, A.K. Recent advancement in wound healing dressing material. *Int. J. Pharm. Sci. Res.* **2019**, *10*, 2572–2577. [CrossRef]
6. Garlotta, D. A literature review of poly(lactic acid). *J. Polym. Environ.* **2001**, *9*, 63–84. [CrossRef]
7. Auras, R.; Lim, L.T.; Selke, S.E.M.; Tsuji, H. *Poly(lactic acid): Synthesis, Structures, Properties, Processing, and Applications*; John Wiley & Sons, Inc.: Hoboken, NJ, USA, 2010. [CrossRef]
8. Lasprilla, A.J.R.; Martinez, G.A.R.; Lunelli, B.H.; Jardini, A.L.; Filho, R.M. Poly-lactic acid synthesis for application in biomedical devices—A review. *Biotechnol. Adv.* **2012**, *30*, 321–328. [CrossRef]
9. Zhou, J.; Han, S.; Dou, Y.; Lu, J.; Wang, C.; He, H.; Li, X.; Zhang, J. Nanostructured poly(l-lactide) matrix as novel platform for drug delivery. *Int. J. Pharm.* **2013**, *448*, 175–188. [CrossRef] [PubMed]
10. Farah, S.; Anderson, D.G.; Langer, R. Physical and mechanical properties of PLA, and their functions in widespread applications—A comprehensive review. *Adv. Drug. Deliv. Rev.* **2016**, *107*, 367–392. [CrossRef]
11. Koh, J.J.; Zhang, X.; He, C. Fully biodegradable Poly(lactic acid)/Starch blends: A review of toughening strategies. *Int. J. Biol. Macromol.* **2018**, *109*, 99–113. [CrossRef] [PubMed]
12. Nofar, M.; Sacligil, D.; Carreau, P.J.; Kamal, M.R.; Heuzey, M.C. Poly (lactic acid) blends: Processing, properties and applications. *Int. J. Biol. Macromol.* **2019**, *125*, 307–360. [CrossRef]
13. Sharif, A.; Mondal, S.; Hoque, M.E. Polylactic acid (PLA)-based nanocomposites: Processing and properties. In *Bio-Based Polymers and Nanocomposites: Preparation, Processing, Properties & Performance*; Springer Nature: Cham, Switzerland, 2019; pp. 233–254.
14. Alam, F.; Shukla, V.R.; Varadarajan, K.M.; Kumar, S. Microarchitected 3D printed polylactic acid (PLA) nanocomposite scaffolds for biomedical applications. *J. Mech. Behav. Biomed. Mater.* **2020**, *103*, 103576. [CrossRef] [PubMed]
15. Kliem, S.; Kreutzbruck, M.; Bonten, C. Review on the biological degradation of polymers in various environments. *Materials* **2020**, *13*, 4586. [CrossRef] [PubMed]
16. Wang, C.-Y.; Makvandi, P.; Zare, E.N.; Tay, F.R.; Niu, L.-N. Advances in antimicrobial organic and inorganic nanocompounds in biomedicine. *Adv. Ther.* **2020**, *3*, 2000024. [CrossRef]
17. Saidin, S.; Jumat, M.A.; Mohd Amin, N.A.A.; Saleh Al-Hammadi, A.S. Organic and inorganic antibacterial approaches in combating bacterial infection for biomedical application. *Mater. Sci. Eng. C* **2021**, *118*, 111382. [CrossRef] [PubMed]
18. Mahltig, B.; Soltmann, U.; Haase, H. Modification of algae with zinc, copper and silver ions for usage as natural composite for antibacterial applications. *Mater. Sci. Eng. C* **2013**, *33*, 979–983. [CrossRef] [PubMed]
19. Kwiczak-Yigitbasi, J.; Lacin, O.; Demir, M.; Ahan, R.E.; Seker, U.O.S.; Baytekin, B. A sustainable preparation of catalytically active and antibacterial cellulose metal nanocomposites: Via ball milling of cellulose. *Green Chem.* **2020**, *22*, 455–464. [CrossRef]
20. Pettinari, C.; Pettinari, R.; Di Nicola, C.; Tombesi, A.; Scuri, S.; Marchetti, F. Antimicrobial MOFs. *Coord. Chem. Rev.* **2021**, *446*, 214121. [CrossRef]
21. Song, J.M. Silver as antibacterial agent: Metal nanoparticles to nanometallopharmaceuticals (Silver based antibacterial nanometallopharmaceuticals). In Proceedings of the 2010 IEEE International Conference on Nano/Molecular Medicine and Engineering, Hung Hom, China, 5–9 December 2010; pp. 98–101.
22. Cheng, Y.-J.; Zeiger, D.N.; Howarter, J.A.; Zhang, X.; Lin, N.J.; Antonucci, J.M.; Lin-Gibson, S. In situ formation of silver nanoparticles in photocrosslinking polymers. *J. Biomed. Mater. Res. Part B Appl. Biomater.* **2011**, *97 B*, 124–131. [CrossRef]
23. Jin, G.; Prabhakaran, M.P.; Nadappuram, B.P.; Sing, G.; Kai, D.; Ramakrishna, S. Electrospun poly(L-lactic acid)-co-poly(ε-caprolactone) nanofibres containing silver nanoparticles for skin-tissue engineering. *J. Biomater. Sci. Polym. Ed.* **2012**, *23*, 2337–2352. [CrossRef]

24. Xie, C.; Lu, X.; Wang, K. Pulse electrochemical synthesis of spherical hydroxyapatite and silver nanoparticles mediated by the polymerization of polypyrrole on metallic implants for biomedical applications. *Part. Part. Syst. Charact.* **2015**, *32*, 630–635. [CrossRef]
25. Wan, C.; Li, J. Cellulose aerogels functionalized with polypyrrole and silver nanoparticles: In-situ synthesis, characterization and antibacterial activity. *Carbohydr. Polym.* **2016**, *146*, 362–367. [CrossRef] [PubMed]
26. Shuai, C.; Xu, Y.; Feng, P.; Wang, G.; Xiong, S.; Peng, S. Antibacterial polymer scaffold based on mesoporous bioactive glass loaded with in situ grown silver. *Chem. Eng. J.* **2019**, *374*, 304–315. [CrossRef]
27. Calamak, S.; Aksoy, E.A.; Ertas, N.; Erdogdu, C.; Sagiroglu, M.; Ulubayram, K. Ag/silk fibroin nanofibers: Effect of fibroin morphology on Ag+ release and antibacterial activity. *Eur. Polym. J.* **2015**, *67*, 99–112. [CrossRef]
28. Duan, C.; Meng, J.; Wang, X.; Meng, X.; Sun, X.; Xu, Y.; Zhao, W.; Ni, Y. Synthesis of novel cellulose- based antibacterial composites of Ag nanoparticles@ metal-organic frameworks@ carboxymethylated fibers. *Carbohydr. Polym.* **2018**, *193*, 82–88. [CrossRef] [PubMed]
29. Xie, C.M.; Lu, X.; Wang, K.F.; Meng, F.Z.; Jiang, O.; Zhang, H.P.; Zhi, W.; Fang, L.M. Silver nanoparticles and growth factors incorporated hydroxyapatite coatings on metallic implant surfaces for enhancement of osteoinductivity and antibacterial properties. *ACS Appl. Mater. Interfaces* **2014**, *6*, 8580–8589. [CrossRef] [PubMed]
30. Dubnika, A.; Loca, D.; Rudovica, V.; Parekh, M.B.; Berzina-Cimdina, L. Functionalized silver doped hydroxyapatite scaffolds for controlled simultaneous silver ion and drug delivery. *Ceram. Int.* **2017**, *43*, 3698–3705. [CrossRef]
31. Li, J.; Kang, L.; Wang, B.; Chen, K.; Tian, X.; Ge, Z.; Zeng, J.; Xu, J.; Gao, W. Controlled release and long-term antibacterial activity of dialdehyde nanofibrillated cellulose/silver nanoparticle composites. *ACS Sustain. Chem. Eng.* **2019**, *7*, 1146–1158. [CrossRef]
32. Jia, Z.; Lv, X.; Hou, Y.; Wang, K.; Ren, F.; Xu, D.; Wang, Q.; Fan, K.; Xie, C.; Lu, X. Mussel-inspired nanozyme catalyzed conductive and self-setting hydrogel for adhesive and antibacterial bioelectronics. *Bioact. Mater.* **2021**, *6*, 2676–2687. [CrossRef] [PubMed]
33. Vaidhyanathan, B.; Vincent, P.; Vadivel, S.; Karuppiah, P.; Abdullah, N.; Deep, A.D.; Sadhasivam, R.; Vimalraj, S.; Saravanan, S. Fabrication and investigation of the suitability of chitosan-silver composite scaffolds for bone tissue engineering applications. *Process Biochem.* **2021**, *100*, 178–187. [CrossRef]
34. Bagchi, B.; Kar, S.; Dey, S.K.; Bhandary, S.; Roy, D.; Mukhopadhyay, T.; Das, S.; Nandy, P. In situ synthesis and antibacterial activity of copper nanoparticle loaded natural montmorillonite clay based on contact inhibition and ion release. *Colloids Surf. B Biointerfaces* **2013**, *108*, 358–365. [CrossRef] [PubMed]
35. Ilnicka, A.; Walczyk, M.; Lukaszewicz, J.P.; Janczak, K.; Malinowski, R. Antimicrobial carbon materials incorporating copper nano-crystallites and their PLA composites. *J. Appl. Polym. Sci.* **2016**, *133*, 43429. [CrossRef]
36. García, A.; Rodríguez, B.; Giraldo, H.; Quintero, Y.; Quezada, R.; Hassan, N.; Estay, H. Copper-modified polymeric membranes for water treatment: A comprehensive review. *Membranes* **2021**, *11*, 93. [CrossRef] [PubMed]
37. Aničić, N.; Kurtjak, M.; Jeverica, S.; Suvorov, D.; Vukomanović, M. Antimicrobial polymeric composites with embedded nanotextured magnesium oxide. *Polymers* **2021**, *13*, 2183. [CrossRef] [PubMed]
38. Scopus Base: 6905 Document Results on Antibacterial Zinc. Available online: https://www-1scopus-1com-100001411012f.han.p.lodz.pl/results/results.uri?sid=94895d0abb0adeb79616d9f4561396f8&src=s&sot=b&sdt=b&origin=searchbasic&rr=&sl=34&s=TITLE-ABS-KEY(Antibacterial%20%20Zinc)&searchterm1=Antibacterial%20%20Zinc&searchTerms=&connectors=&field1=TITLE_ABS_KEY&fields=) (accessed on 11 September 2021).
39. Vallee, B.L.; Falchuk, K.H. The biochemical basis of zinc physiology. *Physiol. Rev.* **1993**, *73*, 79–118. [CrossRef] [PubMed]
40. Fosmire, G.J. Zinc toxicity. *Am. J. Clin. Nutr.* **1990**, *51*, 225–227. [CrossRef] [PubMed]
41. Cheknev, S.B.; Vostrova, E.I.; Apresova, M.A.; Piskovskaya, L.S.; Vostrov, A.V. Deceleration of bacterial growth in *Staphylococcus aureus* and *Pseudomonas aeruginosa* cultures in the presence of copper and zinc cations. *Zhurnal Mikrobiol. Epidemiol. Immunobiol.* **2015**, *2*, 9–17. [PubMed]
42. Jones, N.; Ray, B.; Ranjit, K.T.; Manna, A.C. Antibacterial activity of ZnO nanoparticle suspensions on a broad spectrum of microorganisms. *FEMS Microbiol. Lett.* **2008**, *279*, 71–76. [CrossRef]
43. Hoseinnejad, M.; Jafari, S.M.; Katouzian, I. Inorganic and metal nanoparticles and their antimicrobial activity in food packaging applications. *Crit. Rev. Microbiol.* **2018**, *44*, 161–181. [CrossRef] [PubMed]
44. Yuvasravana, R.; George, P.P.; Devanna, N.; Apsana, G. Fabrication and comparison between anti-bacterial properties of metal oxide nanoparticles prepared by a biogenic approach. *J. Bionanosci.* **2018**, *12*, 408–416. [CrossRef]
45. Li, Y.; Liao, C.; Tjong, S.C. Recent advances in zinc oxide nanostructures with antimicrobial activities. *Int. J. Mol. Sci.* **2020**, *21*, 8836. [CrossRef] [PubMed]
46. Geetha, P. Antibacterial and anticancer activities of biogenic synthesized Ag and ZnO NPS. *Int. J. Innov. Technol. Expl. Eng.* **2019**, *8*, 3143–3147.
47. Hu, H.; Yu, L.; Qian, X.; Chen, Y.; Chen, B.; Li, Y. Chemoreactive nanotherapeutics by metal peroxide based nanomedicine. *Adv. Sci.* **2021**, *8*, 2000494. [CrossRef]
48. Bock, C.W.; Katz, A.K.; Glusker, J.P. Hydration of zinc ions: A comparison with magnesium and beryllium ions. *J. Amer. Chem. Soc.* **1995**, *117*, 3754–3765. [CrossRef]
49. Xia, J.; Shi, Y.; Zhang, Y.; Miao, Q.; Tang, W. Deprotonation of zinc(II)−water and zinc(II)−alcohol and nucleophilicity of the resultant zinc(II) hydroxide and zinc(II) alkoxide in double-functionalized complexes: Theoretical studies on models for hydrolytic zinc enzymes. *Inorg. Chem.* **2003**, *42*, 70–77. [CrossRef]

50. Maret, W. Zinc and human disease. *Met. Ions Life Sci.* **2013**, *13*, 389–414. [CrossRef]
51. Krezel, A.; Maret, W. The biological inorganic chemistry of zinc ions. *Arch. Biochem. Biophys.* **2016**, *611*, 3–19. [CrossRef] [PubMed]
52. Ogawa, Y.; Kawamura, T.; Shimadaet, S. Zinc and skin biology. *Arch. Biochem. Biophys.* **2016**, *611*, 113–119. [CrossRef] [PubMed]
53. Abendrot, M.; Chęcińska, L.; Kusz, J.; Lisowska, K.; Zawadzka, K.; Felczak, A.; Kalinowska-Lis, U. Zinc(II) complexes with amino acids for potential use in dermatology: Synthesis, crystal structures, and antibacterial activity. *Molecules* **2020**, *25*, 951. [CrossRef] [PubMed]
54. Pellei, M.; Del Bello, F.; Porchia, M.; Santini, C. Zinc coordination complexes as anticancer agents. *Coord. Chem. Rev.* **2021**, *445*, 214088. [CrossRef]
55. Dudev, T.; Lim, C. Tetrahedral vs. octahedral zinc complexes with ligands of biological interest: A DFT/CDM study. *J. Am. Chem. Soc.* **2000**, *122*, 11146–11153. [CrossRef]
56. Durrant, P.J.; Durrant, B. *Introduction to Advanced Inorganic Chemistry*; Longman, Green &Co Ltd.: London, UK, 1962; pp. 508–522. ISBN 0582442133.
57. Sthoer, A.; Hladılkova, J.; Lund, M.; Tyrode, E. Molecular insight into carboxylic acid–alkali metal cations interactions: Reversed affinities and ion-pair formation revealed by non-linear optics and simulations. *Phys. Chem. Chem. Phys.* **2019**, *21*, 11329–11344. [CrossRef] [PubMed]
58. Draget, K.L.; Taylor, C. Chemical, physical and biological properties of alginates and their biomedical implications. *Food Hydrocoll.* **2011**, *25*, 251–256. [CrossRef]
59. Lee, K.Y.; Mooney, D.J. Alginate: Properties and biomedical applications. *Prog. Polym. Sci.* **2012**, *37*, 106–126. [CrossRef] [PubMed]
60. Pawar, S.N.; Edgar, K.J. Alginate derivatization: A review of chemistry, properties and applications. *Biomaterials* **2012**, *33*, 3279–3305. [CrossRef]
61. Fernando, I.P.S.; Kim, D.; Nah, J.W.; Jeon, Y.J. Advances in functionalizing fucoidans and alginates (bio)polymers by structural modifications: A review. *Chem. Eng. J.* **2019**, *355*, 33–48. [CrossRef]
62. Zhang, C.; Show, P.-L.; Ho, S.-H. Progress and perspective on algal plastics—A critical review. *Bioresour. Technol.* **2019**, *289*, 121700. [CrossRef] [PubMed]
63. Kuznetsova, T.A.; Andryukov, B.G.; Besednova, N.N.; Zaporozhets, T.S.; Kalinin, A.V. Marine algae polysaccharides as basis for wound dressings, drug delivery, and tissue engineering: A review. *J. Mar. Sci. Eng.* **2020**, *8*, 481. [CrossRef]
64. Scopus Base: 5294 Documents Results on Alginates for Drug Delivery. Available online: https://www-1scopus-1com-10000145y03aa.han.p.lodz.pl/results/results.uri?sid=4ed83aab7077f9b156f7eba71e34db0d&src=s&sot=b&sdt=b&origin=searchbasic&rr=&sl=41&s=TITLE-ABS-KEY(alginate%20for%20drug%20delivery)&searchterm1=alginate%20for%20drug%20delivery&searchTerms=&connectors=&field1=TITLE_ABS_KEY&fields= (accessed on 1 September 2021).
65. Gholamali, I.; Yadollahi, M. Bio-nanocomposite polymer hydrogels containing nanoparticles for drug delivery: A Review. *Regen. Eng. Transl. Med.* **2021**, *7*, 129–146. [CrossRef]
66. Jana, P.; Shyam, M.; Singh, S.; Jayaprakash, V.; Dev, A. Biodegradable polymers in drug delivery and oral vaccination. *Eur. Polym. J.* **2021**, *142*, 110155. [CrossRef]
67. Salamanna, F.; Gambardella, A.; Contartese, D.; Visani, A.; Fini, M. Nano-based biomaterials as drug delivery systems against osteoporosis: A systematic review of preclinical and clinical evidence. *Nanomaterials* **2021**, *11*, 530. [CrossRef] [PubMed]
68. Li, M.; Sun, Y.; Ma, C.; Hua, Y.; Zhang, L.; Shen, J. Design and investigation of penetrating mechanism of octaarginine-modified alginate nanoparticles for improving intestinal insulin delivery. *J. Pharm. Sci.* **2021**, *110*, 268–279. [CrossRef]
69. Volpatti, L.R.; Facklam, A.L.; Cortinas, A.B.; Lu, Y.C.; Matranga, M.A.; MacIsaac, C.; Hill, M.C.; Langer, R.; Anderson, D.G. Microgel encapsulated nanoparticles for glucose-responsive insulin delivery. *Biomaterials* **2021**, *267*, 120458. [CrossRef] [PubMed]
70. Bulut, E. Development and optimization of Fe^{3+}-crosslinked sodium alginate-methylcellulose semi-interpenetrating polymer network beads for controlled release of ibuprofen. *Int. J. Biol. Macromol.* **2021**, *168*, 823–883. [CrossRef] [PubMed]
71. Freitas, E.D.; Freitas, V.M.S.; Rosa, P.C.P.; da Silva, M.G.C.; Vieira, M.G.A. Development and evaluation of naproxen-loaded sericin/alginate beads for delayed and extended drug release using different covalent crosslinking agents. *Mater. Sci. Eng. C* **2021**, *118*, 111412. [CrossRef] [PubMed]
72. Santinon, C.; Dantas de Freitas, E.; Gurgel Carlos da Silva, M.; Gurgel Adeodato Vieira, M. Modification of valsartan drug release by incorporation into sericin/alginate blend using experimental design methodology. *Eur. Polym. J.* **2021**, *153*, 110506. [CrossRef]
73. Jing, C.; Li, B.; Tan, H.; Zhang, C.; Liang, H.; Na, H.; Chen, S.; Liu, C.; Zhao, L. Alendronate-decorated nanoparticles as bone-targeted alendronate carriers for potential osteoporosis treatment. *ACS Appl. Bio Mater.* **2021**, *4*, 4907–4916. [CrossRef]
74. Lakkakula, J.R.; Gujarathi, P.; Pansare, P.; Tripathi, S. A comprehensive review on alginate-based delivery systems for the delivery of chemotherapeutic agent: Doxorubicin. *Carbohydr. Polym.* **2021**, *259*, 117696. [CrossRef] [PubMed]
75. Mallakpour, S.; Azadi, E.; Hussain, C.M. Chitosan, alginate, hyaluronic acid, gums, and β-glucan as potent adjuvants and vaccine delivery systems for viral threats including SARS-CoV-2: A review. *Int. J. Biol. Macromol.* **2021**, *182*, 1931–1940. [CrossRef] [PubMed]
76. Song, M.; Xia, W.; Tao, Z.; Zhu, B.; Zhang, W.; Liu, C.; Chen, S. Self-assembled polymeric nanocarrier-mediated co-delivery of metformin and doxorubicin for melanoma therapy. *Drug Deliv.* **2021**, *28*, 594–606. [CrossRef]
77. Sreekanth Reddy, O.; Subha, M.C.S.; Jithendra, T.; Madhavi, C.; Chowdoji Rao, K. Curcumin encapsulated dual cross linked sodium alginate/montmorillonite polymeric composite beads for controlled drug delivery. *J. Pharm. Anal.* **2021**, *11*, 191–199. [CrossRef] [PubMed]

78. Sun, H.; Zhang, C.; Zhang, B.; Song, P.; Xu, X.; Gui, X.; Chen, X.; Lu, G.; Li, X.; Liang, J.; et al. 3D printed calcium phosphate scaffolds with controlled release of osteogenic drugs for bone regeneration. *Chem. Eng. J.* **2022**, *427*, 130961. [CrossRef]
79. Scopus Base: 3749 Document Results on Alginates in Tissue Engineering. Available online: https://www-1scopus-1com-10000145y0303.han.p.lodz.pl/results/results.uri?sid=dbef89d705f695750247b64d1f980f7b&src=s&sot=b&sdt=b&origin=searchbasic&rr=&sl=46&s=TITLE-ABS-KEY(alginate%20for%20tissue%20engineering)&searchterm1=alginate%20for%20tissue%20engineering&searchTerms=&connectors=&field1=TITLE_ABS_KEY&fields= (accessed on 1 September 2021).
80. Sahoo, D.R.; Biswal, T. Alginate and its application to tissue engineering. *SN Appl. Sci.* **2021**, *3*, 30. [CrossRef]
81. Kohli, N.; Sharma, V.; Orera, A.; Sawadkar, P.; Owji, N.; Frost, O.G.; Bailey, R.J.; Snow, M.; Knowles, J.C.; Blunn, G.W.; et al. Pro-angiogenic and osteogenic composite scaffolds of fibrin, alginate and calcium phosphate for bone tissue engineering. *J. Tissue Eng.* **2021**, *12*, 20417314211005610. [CrossRef] [PubMed]
82. Sathain, A.; Monvisade, P.; Siriphannon, P. Bioactive alginate/carrageenan/calcium silicate porous scaffolds for bone tissue engineering. *Mater. Today Commun.* **2021**, *26*, 102165. [CrossRef]
83. Naranda, J.; Bračič, M.; Vogrin, M.; Maver, U. Recent advancements in 3d printing of polysaccharide hydrogels in cartilage tissue engineering. *Materials* **2021**, *14*, 3977. [CrossRef] [PubMed]
84. Pushp, P.; Gupta, M.K. Cardiac tissue engineering: A role for natural biomaterials. In *Bioactive Natural Products for Pharmaceutical Applications*; Advanced Structured Materials; Pal, D., Nayak, A.K., Eds.; Springer: Cham, Switzerland, 2021; Volume 140. [CrossRef]
85. Boulais, L.; Jellali, R.; Pereira, U.; Leclerc, E.; Bencherif, S.A.; Legallais, C. Cryogel-integrated biochip for liver tissue engineering. *ACS Appl. Bio Mater.* **2021**, *4*, 5617–5626. [CrossRef]
86. Shulimzon, T.R.; Giladi, S.; Zilberman, M. Catheter injectable hydrogel-based scaffolds for tissue engineering applications in lung disease. *Isr. Med. Assoc. J.* **2021**, *22*, 736–740. [PubMed]
87. Campiglio, C.E.; Carcano, A.; Draghi, L. RGD-pectin microfiber patches for guiding muscle tissue regeneration. *J. Biomed. Mater. Res. Part A* **2021**, in press. [CrossRef] [PubMed]
88. Ghaderinejad, P.; Najmoddin, N.; Bagher, Z.; Saeed, M.; Karimi, S.; Simorgh, S.; Pezeshki-Modaress, M. An injectable anisotropic alginate hydrogel containing oriented fibers for nerve tissue engineering. *Chem. Eng. J.* **2021**, *420*, 130465. [CrossRef]
89. Barros, N.R.; Kim, H.-J.; Gouidie, M.J.; Lee, K.J.; Bandaru, P.; Banton, E.A.; Sarikhani, E.; Sun, W.; Zhang, S.; Cho, H.J.; et al. Biofabrication of endothelial cell, dermal fibroblast, and multilayered keratinocyte layers for skin tissue engineering. *Biofabrication* **2021**, *13*, 035030. [CrossRef] [PubMed]
90. Scopus Base: 1392 Document Results on Alginates in Tissue Engineering. Available online: https://www-1scopus-1com-10000145y0316.han.p.lodz.pl/results/results.uri?sid=33b3b9f2600cb7bbc5975c67d12053da&src=s&sot=b&sdt=b&origin=searchbasic&rr=&sl=43&s=TITLE-ABS-KEY(alginate%20for%20wound%20dressings)&searchterm1=alginate%20for%20wound%20dressings&searchTerms=&connectors=&field1=TITLE_ABS_KEY&fields= (accessed on 1 September 2021).
91. Arora, S.; Nagpal, M.; Kaur, M. Recent updates on biopolymers based wound dressings. *Asian J. Chem.* **2021**, *33*, 1457–1470. [CrossRef]
92. Azhar, F.F.; Rostamzadeh, P.; Khordadmehr, M.; Mesgari-Abbasi, M. Evaluation of a novel bioactive wound dressing: An in vitro and in vivo study. *J. Wound Care* **2021**, *30*, 482–490. [CrossRef] [PubMed]
93. Jing, X.; Sun, Y.; Ma, X.; Hu, H. Marine polysaccharides: Green and recyclable resources as wound dressings. *Mater. Chem. Front.* **2021**, *5*, 5595–5616. [CrossRef]
94. Garcia, T.F.; Silva, P.G.A.; Barcelos, B.J.; Miranda, M.G.R.; Alonso, C.S.; Abreu, M.N.S.; Borges, E.L. Criteria to evaluate the quality of alginate wound dressings. *Rev. Bras. Enferm.* **2021**, *74*, e20201091. [CrossRef] [PubMed]
95. De Luca, I.; Pedram, P.; Moeini, A.; Cerruti, P.; Peluso, G.; Di Salle, A.; Germann, N. Nanotechnology development for formulating essential oils in wound dressing materials to promote the wound-healing process: A review. *Appl. Sci.* **2021**, *11*, 1713. [CrossRef]
96. Kibungu, C.; Kondiah, P.P.D.; Kumar, P.; Choonara, Y.E. This review recent advances in chitosan and alginate-based hydrogels for wound healing application. *Front. Mater.* **2021**, *8*, 681960. [CrossRef]
97. Weng, L.; Zhang, X.; Fan, W.; Lu, Y. Development of the inorganic nanoparticles reinforced alginate-based hybrid fiber for wound care and healing. *J. Appl. Polym. Sci.* **2021**, *138*, 51228. [CrossRef]
98. Shen, H.Y.; Liu, Z.-H.; Hong, J.-S.; Wu, M.S.; Shiue, S.-J.; Lin, H.-Y. Controlled-release of free bacteriophage nanoparticles from 3D-plotted hydrogel fibrous structure as potential antibacterial wound dressing. *J. Control. Release* **2021**, *331*, 154–163. [CrossRef] [PubMed]
99. Li, J.; He, J.; Huang, Y. Role of alginate in antibacterial finishing of textiles. *Int. J. Biol. Macromol.* **2017**, *94*, 466–473. [CrossRef] [PubMed]
100. Caterson, E.J.; Nesti, L.J.; Li, W.-J.; Danielson, K.G.; Albert, T.J.; Vaccaro, A.R.; Tuan, R.S. Three-dimensional cartilage formation by bone marrow-derived cells seeded in polylactide/alginate amalgam. *J. Biomed. Mater. Res.* **2001**, *57*, 394–403. [CrossRef]
101. Caterson, E.J.; Li, W.J.; Nesti, L.J.; Albert, T.; Danielson, K.; Tuan, R.S. Polymer/alginate amalgam for cartilage-tissue engineering. *Ann. N. Y. Acad. Sci.* **2002**, *961*, 134–138. [CrossRef] [PubMed]
102. Wayne, J.S.; McDowell, C.L.; Shields, K.J.; Tuan, R.S. In vivo response of polylactic acid-alginate scaffolds and bone marrow-derived cells for cartilage tissue engineering. *Tissue Eng.* **2005**, *11*, 953–963. [CrossRef] [PubMed]
103. Kessler, M.; Esser, E.; Groll, J.; Tessmar, J. Bilateral PLA/alginate membranes for the prevention of postsurgical adhesions. *J. Biomed. Mater. Res. Part B Appl. Biomater.* **2016**, *104*, 1563–1570. [CrossRef] [PubMed]

104. Wu, H.; Liu, J.; Fang, Q.; Xiao, B.; Wan, Y. Establishment of nerve growth factor gradients on aligned chitosan-polylactide /alginate fibers for neural tissue engineering applications. *Colloids Surf. B Biointerfaces* **2017**, *160*, 598–609. [CrossRef] [PubMed]
105. Yang, M.; Yang, T.; Jia, J.; Lu, T.; Wang, H.; Yan, X.; Wang, L.; Yu, L.; Zhao, Y. Fabrication and characterization of DDAB/PLA-alginate composite microcapsules as single-shot vaccine. *RSC Adv.* **2018**, *8*, 13612–13624. [CrossRef]
106. Pandey, G.; Chaudhari, R.; Joshi, B.; Choudhary, S.; Kaur, J.; Joshi, A. Fluorescent biocompatible platinum-porphyrin–doped polymeric hybrid particles for oxygen and glucose biosensing. *Sci. Rep.* **2019**, *9*, 5029. [CrossRef] [PubMed]
107. Li, X.; Saeed, S.S.; Beni, M.H.; Morovvati, M.R.; Angili, S.N.; Toghraie, D.; Khan, A. Experimental measurement and simulation of mechanical strength and biological behavior of porous bony scaffold coated with alginate-hydroxyapatite for femoral applications. *Comp. Sci. Technol.* **2021**, *214*, 108973. [CrossRef]
108. Yokoyama, F.; Achife, C.E.; Takahira, K.; Yamashita, Y.; Monobe, K.; Kusano, F.; Nishi, K. Morphologies of oriented alginate gels crosslinked with various divalent metal ions. *J. Macromol. Sci. Part B* **1992**, *31*, 463–483. [CrossRef]
109. Pistone, S.; Qoragllu, D.; Smistad, G.; Hiorth, M. Formulation and preparation of stable cross-linked alginate-zinc nanoparticles in the presence of a monovalent salt. *Soft Matter* **2015**, *11*, 5765–5774. [CrossRef] [PubMed]
110. Pérez-Madrigal, M.M.; Torras, J.; Casanovas, J.; Haring, M.; Alemán, C.; Díaz, D.D. Paradigm shift for preparing versatile M2+-free gels from unmodified sodium alginate. *Biomacromolecules* **2017**, *18*, 2967–2979. [CrossRef]
111. Frígols, B.; Martí, M.; Salesa, B.; Hernández-Oliver, C.; Aarstad, O.; Teialeret Ulset, A.-S.; Sætrom, G.I.; Aachmann, F.L.; Serrano-Aroca, A. Graphene oxide in zinc alginate films: Antibacterial activity, cytotoxicity, zinc release, water sorption/diffusion, wettability and opacity. *PLoS ONE* **2019**, *14*, e0212819. [CrossRef] [PubMed]
112. Scopus Base: 792 Document Results on Zinc Alginate. Available online: https://www-1scopus-1com-100001411053a.han.p.lodz.pl/results/results.uri?sid=0c7262af62088e8c85153ce6d35be38c&src=s&sot=b&sdt=b&origin=searchbasic&rr=&sl=28&s=TITLE-ABS-KEY(zinc%20alginate)&searchterm1=zinc%20alginate&searchTerms=&connectors=&field1=TITLE_ABS_KEY&fields= (accessed on 1 September 2021).
113. Jang, L.K.; Nguyen, D.; Geesey, G.G. An equilibrium model for absorption of multiple divalent metals by alginate gel under acidic conditions. *Water Res.* **1999**, *33*, 2826–2832. [CrossRef]
114. Chan, L.W.; Jin, Y.; Heng, P.W.S. Cross-linking mechanisms of calcium and zinc in production of alginate microspheres. *Int. J. Pharm.* **2002**, *242*, 255–258. [CrossRef]
115. Lai, Y.L.; Annadurai, G.; Huang, F.C.; Lee, J.F. Biosorption of Zn(II) on the different Ca-alginate beads from aqueous solution. *Bioresour. Technol.* **2008**, *99*, 6480–6487. [CrossRef]
116. Lai, Y.L.; Thirumavalavan, M.; Lee, J.F. Effective adsorption of heavy metal ions (Cu^{2+}, Pb^{2+}, Zn^{2+}) from aqueous solution by immobilization of adsorbents on Ca-alginate beads. *Toxicol. Environ. Chem.* **2010**, *92*, 697–705. [CrossRef]
117. Plazinski, W.; Drach, M. Binding of bivalent metal cations by α-l-guluronate: Insights from the DFT-MD simulations. *New J. Chem.* **2015**, *39*, 3987–3994. [CrossRef]
118. Zhou, Q.; Kang, H.; Bielec, M.; Wu, X.; Cheng, Q.; Wei, W.; Dai, H. Influence of different divalent ions cross-linking sodium alginate-polyacrylamide hydrogels on antibacterial properties and wound healing. *Carbohydr. Polym.* **2018**, *197*, 292–304. [CrossRef]
119. Iskandar, L.; Rojo, L.; Di Silvio, L.; Deb, S. The effect of chelation of sodium alginate with osteogenic ions, calcium, zinc, and strontium. *J. Biomater. Appl.* **2019**, *34*, 573–584. [CrossRef] [PubMed]
120. Cardoso, S.L.; Costa, C.S.D.; Da Silva, M.G.C.; Vieira, M.G.A. Insight into zinc(II) biosorption on alginate extraction residue: Kinetics, isotherm and thermodynamics. *J. Environ. Chem. Eng.* **2020**, *8*, 103629. [CrossRef]
121. Lucaci, A.R.; Bulgariu, D.; Ahmad, I.; Bulgariu, L. Equilibrium and kinetics studies of metal ions biosorption on alginate extracted from marine red algae biomass (*Callithamnion corymbosum* sp.). *Polymers* **2020**, *12*, 1888. [CrossRef] [PubMed]
122. Cendon, F.V.; Salomão, B.B.; Jorge, R.M.M.; Mathias, A.L. Mechanical and optical evaluation of alginate hydrospheres produced with different cross-linking salts for industrial application. *Colloid Polym. Sci.* **2021**, *299*, 693–703. [CrossRef]
123. Hu, C.; Lu, W.; Mata, A.; Nishinari, K.; Fang, Y. Ions-induced gelation of alginate: Mechanisms and applications. *Int. J. Biol. Macromol.* **2021**, *177*, 578–588. [CrossRef]
124. Sutirman, Z.A.; Sanagi, M.M.; Wan Aini, W.I. Alginate-based adsorbents for removal of metal ions and radionuclides from aqueous solutions: A review. *Int. J. Bio. Macromol.* **2021**, *174*, 216–228. [CrossRef]
125. Kudzin, M.H.; Mrozińska, Z.; Walawska, A.; Sójka-Ledakowicz, J. Biofunctionalization of textile materials. 1. Biofunctionalization of poly(propylene) (PP) nonwovens fabrics by Alafosfalin. *Coatings* **2019**, *9*, 412. [CrossRef]
126. Kudzin, M.H.; Mrozińska, Z. Biofunctionalization of textile materials. 2. Antimicrobial modification of poly(lactide) (PLA) nonwoven fabrics by fosfomycin. *Polymers* **2020**, *12*, 768. [CrossRef] [PubMed]
127. Kudzin, M.H.; Mrozińska, Z. Biofunctionalization of textile materials.3. Biofunctionalization of poly(lactide) (PLA) nonwovens fabrics by KI. *Coatings* **2020**, *10*, 593. [CrossRef]
128. Sójka-Ledakowicz, J.; Kudzin, M.H. Effect of plasma modification on the chemical structure of a polyethylene terephthalate fabrics surface. *Fibres Text. East. Eur.* **2014**, *22*, 118–122.
129. Kudzin, M.H.; Mrozinska, Z.; Kaczmarek, A.; Lisiak-Kucinska, A. Deposition of copper on poly(lactide) non-woven fabrics by magnetron sputtering–fabrication of new multi-functional, antimicrobial composite. *Materials* **2020**, *13*, 3971. [CrossRef] [PubMed]

130. Kudzin, M.H.; Kaczmarek, A.; Mrozińska, Z.; Olczyk, J. Deposition of copper on polyester knitwear fibers by a magnetron sputtering system. Physical properties, and evaluation of antimicrobial response of new multi-functional composite materials. *Appl. Sci.* **2020**, *10*, 6990. [CrossRef]
131. Kudzin, M.H.; Boguń, M.; Mrozińska, Z.; Kaczmarek, A. Physical properties, chemical analysis, and evaluation of antimicrobial response of new polylactide/alginate/copper composite materials. *Mar. Drugs* **2020**, *18*, 660. [CrossRef] [PubMed]
132. Kudzin, M.H.; Mrozi´nska, Z.; Urbaniak, P. Vapor phosphorylation of cellulose by phosphorus TrichloRide: Selective phosphorylation of 6-hydroxyl function—The synthesis of new antimicrobial cellulose 6-phosphate(III)-copper complexes. *Antibiotics* **2021**, *10*, 203. [CrossRef] [PubMed]
133. Stańczyk, B.; Dobrzański, L.; Góra, K.; Jach, K.; Jagoda, A. Hydrophobic organic layers on smooth and 3-dimensional developed surfaces. *Electron. Mater.* **2015**, *43*, 3.
134. Analytical Methods for Atomic Absorption Spectroscopy. The Perkin-Elmer Corporation, 1996. Available online: www1.lasalle.edu/ (accessed on 3 July 2020).
135. EN ISO 20645:2006. *Textile Fabrics. Determination of Antibacterial Activity—Agar Diffusion Plate Test*; International Organization for Standardization: Geneva, Switzerland, 2006.
136. EN 14119: 2005 Point 10.5 (B2). *Testing of Textiles. Evaluation of the Action of Microfungi. Visual Method*; International Organization for Standardization: Geneva, Switzerland, 2005.